THE JOURNAL OF BIOLOGICAL CHEMISTRY VOL. 291, NO. 8, pp. 3682–3692, February 19, 2016

Gain-of-Function Mutation W493R in the Epithelial Sodium Channel Allosterically Reconfigures Intersubunit Coupling*[S]◆

Received for publication, July 10, 2015, and in revised form, December 1, 2015 Published, JBC Papers in Press, December 14, 2015, DOI 10.1074/jbc.M115.678052

Mahmoud Shobair[‡§¶], Onur Dagliyan[‡¶1], Pradeep Kota[‡¶], Yan L. Dang[‖], Hong He[‖], M. Jackson Stutts[‖], and Nikolay V. Dokholyan[‡§¶‖2]

From the [‡]Program in Molecular and Cellular Biophysics, [§]Curriculum in Bioinformatics and Computational Biology, [¶]Department of Biochemistry and Biophysics, and [‖]Cystic Fibrosis and Pulmonary Diseases Research and Treatment Center, University of North Carolina at Chapel Hill, Chapel Hill, North Carolina 27599

Sodium absorption in epithelial cells is rate-limited by the epithelial sodium channel (ENaC) activity in lung, kidney, and the distal colon. Pathophysiological conditions, such as cystic fibrosis and Liddle syndrome, result from water-electrolyte imbalance partly due to malfunction of ENaC regulation. Because the quaternary structure of ENaC is yet undetermined, the bases of pathologically linked mutations in ENaC subunits α, β, and γ are largely unknown. Here, we present a structural model of heterotetrameric ENaC $\alpha_1\beta\alpha_2\gamma$ that is consistent with previous cross-linking results and site-directed mutagenesis experiments. By using this model, we show that the disease-causing mutation αW493R rewires structural dynamics of the intersubunit interfaces $\alpha_1\beta$ and $\alpha_2\gamma$. Changes in dynamics can allosterically propagate to the channel gate. We demonstrate that cleavage of the γ-subunit, which is critical for full channel activation, does not mediate activation of ENaC by αW493R. Our molecular dynamics simulations led us to identify a channel-activating electrostatic interaction between α_2Arg-493 and γGlu-348 at the $\alpha_2\gamma$ interface. By neutralizing a sodium-binding acidic patch at the $\alpha_1\beta$ interface, we reduced ENaC activation of αW493R by more than 2-fold. By combining homology modeling, molecular dynamics, cysteine cross-linking, and voltage clamp experiments, we propose a dynamics-driven model for the gain-of-function in ENaC by αW493R. Our integrated computational and experimental approach advances our understanding of structure, dynamics, and function of ENaC in its disease-causing state.

The epithelial sodium channel (ENaC)[3] regulates Na^+ absorption by epithelia, thereby maintaining essential water-electrolyte balance (1, 2). Therefore, altered ENaC activity contributes to pathological conditions that are partly mediated by sodium transport dysregulation, such as cystic fibrosis and Liddle syndrome (1). ENaC is composed of structurally homologous subunits α, β, and γ. Mutations in the α-subunit, such as the gain-of-function mutation αW493R in exon 10, decrease lung functionality (3–7). Carrying the αW493R polymorphism in αENaC can result in chronic bronchitis (4). Heterologous expression of αW493R with β and γ subunits in *Xenopus* oocytes produced an ~4-fold increase in ENaC-mediated current and an increase in the channel open probability (8). However, the structural determinants of this activation remain unknown.

Wild type ENaC is normally proteolytically activated by intracellular furin-like convertases and extracellular trypsin-like serine proteases (9–12). Cleavage of an inhibitory fragment in the finger domain of the α-subunit is thought to reorganize the extracellular domains to favor active conformations of the channel (13). Kashlan *et al.* (13) have elucidated the mechanism of inhibition by the cleaved fragment using synthetic peptides derived from the inhibitory tract of the α-subunit. Releasing the inhibitory tract by proteolysis was found to activate ENaC by eliminating interactions at the thumb and finger domains of the α-subunit. Moreover, previous computational studies on the mechanism of cleavage of ENaC by furin suggest high intrinsic disorder at the furin cleavage sites (9). However, the sequence of proteolytic events and conformational changes leading to channel activation by proteases are still unclear.

Structure-guided design of inhibitors for ENaC has been challenged by a lack of structures for ENaC subunits. In the ENaC/Degenerin family, only the acid-sensing ion channel (ASIC) has been crystalized as a homotrimer in different biophysical states, *i.e.* pH- and toxin-stimulated (14–16). However, functional data show heteromeric assembly of different ASIC subunits. ASICs can exhibit alternative cation permeation functionality by heteromeric assembly of ASIC2a and ASIC2b subunits (17). Although ASIC and ENaC subunits can assemble to form hybrid channels (18), fully functional ENaC oligomers can form only by the assembly of the α-, β-, and γ-subunits. However, channels composed of only α, α and β, or α and γ can still conduct sodium (12). Recently, α-like subunits, δ and ϵ, have been discovered; however, their physiological roles have not been characterized fully (19, 20). Functional data obtained in *Xenopus* oocytes support an oligomeric model of ENaC in which one β-, one γ-, and two α-subunits line the pore (21). Moreover, biochemical analysis of epithelial tissues iso-

* This work was supported by National Institutes of Health Program Project Grant P01 HL 110873-04. The authors declare that they have no conflicts of interest with the contents of this article. The content is solely the responsibility of the authors and does not necessarily represent the official views of the National Institutes of Health.
◆ This article was selected as a Paper of the Week.
[S] This article contains supplemental movies.
[1] A Howard Hughes Medical Institute International Student Research Fellow.
[2] To whom correspondence should be addressed: Biochemistry and Biophysics, University of North Carolina, Chapel Hill, NC 27599-7260. Tel.: 919-843-2513; E-mail: dokh@unc.edu.
[3] The abbreviations used are: ENaC, epithelial sodium channel; ASIC, acid-sensing ion channel; DMD, discrete molecular dynamics; cASIC, chicken ASIC; M2M, 1,2-ethanediyl bismethanethiosulfonate; RMSF, root mean square fluctuation.

lated from rabbit colon and cultured kidney cells indicates a heterotetrameric stoichiometry (22). In contrast, atomic force microscopy studies suggest a heterotrimeric architecture of ENaC (23). The physiological relevance of *in vitro* heteromeric assembly of ENaC is unclear because proper assembly of the α-, β-, and γ-subunits in epithelial cells requires trafficking and sorting machinery (24, 25). Consequently, the stoichiometries of physiologically relevant ENaC oligomers remain uncertain.

These conflicting findings raise the following question. How reliable are classical structure determination techniques in identifying physiologically relevant molecular species? We have combined computational modeling, cysteine cross-linking, and electrophysiology experiments to derive structural evidence for tetrameric ENaC with configuration $\alpha_1\beta\alpha_2\gamma$. In support of previous findings, we propose a dynamics-driven model of ENaC activation by the gain-of-function mutation αW493R; in this model, proteolysis of the γ-subunit is not the major determinant of activation.

Experimental Procedures

Building the Heterotetramer $\alpha_1\beta\alpha_2\gamma$ Model by Symmetric Docking—Previously, we built a homology model of the rat ENaC γ-subunit based on the crystal coordinates of a homolog of ENaC, chicken acid-sensing ion channel cASIC (1, 26). We used the same homology-based approach to construct structural models of the α- and β-subunits. We used our in-house suite MEDUSA for threading ENaC subunit sequences on ASIC structure (27, 28). Alignments of ASIC and ENaC subunits indicated non-homologous insertions and deletions. We used MODELLER to model non-homologous sequences as loops (29). These fragments were then ligated into the homology models designed by MEDUSA and minimized by short discrete molecular dynamics simulations (DMD) (30–33). Briefly, DMD is an event-driven sampling engine that is faster than traditional molecular dynamics under conditions that do not rely on specific solute-solvent interactions. DMD has been successfully used to probe protein dynamics and design molecular switches (34–36).

Because of the lack of a tetrameric template in the ENaC/Degenerin family, we employed symmetric docking using the docking program SymmDock to construct possible tetrameric interfaces of the tetramer $\alpha_1\beta\alpha_2\gamma$ (37). First, we built a homotetrameric model of the α-subunit. Using this homotetramer, we performed structural alignments of the homology models for the β- and γ-subunits according to the configuration $\alpha_1\beta\alpha_2\gamma$. Finally, we used DMD to minimize and relax the model for production run simulations. SymmDock samples the homo-oligomeric configurational space with symmetry C_n from a single monomer using a rigid body docking algorithm with symmetric constraints (37). SymmDock utilizes geometric complementarity of molecular surfaces to symmetrically dock atomic patches. Similar to most docking protocols, the algorithm consists of three stages as follows: molecular representation, patch matching, and model clustering and filtering. Models of oligomeric interfaces are grouped into clusters by two geometric metrics: the direction of axis of symmetry and the projection of center of mass of the asymmetric unit on the axis of symmetry. Clusters are then ranked according to the number of patch-matching pairs pointing to the same axis of symmetry. From the top 100 models ranked by SymmDock's score, one model formed interfaces that correctly arranged the extended conformations of the selectivity filter sequences αGSS, βGGS, and γSCS in a rhombus-like architecture. One drawback of SymmDock is the lack of a post-docking refinement step, which relieves the docked model from steric clashes and re-optimizes side chain geometric complementarity. Therefore, we utilized our in-house developed computational protocols of short DMD simulations for structural refinement. The DMD minimization protocol is publicly available on our Chiron server (38). Chiron can eliminate infinite energy atomic interactions that resemble nonphysical van der Waals volume overlap. Chiron uses a series of short discrete molecular dynamics simulations to overcome interatomic clashes. Briefly, Chiron minimization protocol utilizes a high heat exchange rate $r > 0.2$ fs^{-1} with the thermodynamic bath, which is briefly set to be at a high temperature $T >$ 0.5 DMD reduced unit, ~250 °C (27). By rapidly equilibrating the system at a high thermal energy, Chiron quenches infinite energy interactions.

DMD Protocols for $\alpha_1\beta\alpha_2\gamma$ Minimization and Production Run Simulations—Atomic clashes can be difficult to resolve, especially in hetero-oligomeric complexes, due to the variability in molecular surface complementarity at heteromeric interfaces. In this study, we found that adding a hard harmonic potential with force constant $k > 1$ kcal mol^{-1} Å^{-2} to all backbone atoms helps in equilibrating the system. Because there are four different interfaces in the heterotetramer $\alpha_1\beta\alpha_2\gamma$, additional refinement steps were needed to resolve all steric clashes. First, we conducted a brief packing simulation, 1000 DMD time steps, at heat exchange rate 100 fs^{-1} and temperature 0.1, while keeping the backbone rigid by defining infinite mass to backbone atoms. Following packing, we utilized a combination of relaxation steps similar to steepest descent protocols. Keeping the temperature at 0.1, we assigned a harmonic potential of 5 kcal mol^{-1} Å^{-2} to the Cα atoms. Then, we increased the temperature to 0.3 and equilibrated the system by decreasing the heat exchange coefficient to 0.1 fs^{-1}. Finally, we performed relaxation under unconstrained conditions. The system is ready for production run after minimizing its energy to a stable state. We used our in-house suite MEDUSA to substitute in our relaxed model Trp-493 for Arg-493 in the human α-subunit sequence (39). To simulate the structural dynamics of the constructed and minimized heterotetramer in wild type and mutant states, we assigned soft harmonic constraints to all backbone atoms of the two transmembrane domains (TM1 and TM2) in all subunits to mimic protein-lipid interactions. The applied harmonic potential had a force constant of 0.1 kcal mol^{-1} Å^{-2}. This parameter allowed the transmembrane backbone atoms to sample more confined configurations than the sampled conformations of the solvent-exposed extracellular domains.

Molecular Biology and Biochemistry—Full-length cDNAs of hENaC subunits were cloned from pcDNA plasmids into the pSDE vector for cRNA synthesis and electrophysiology recording of ENaC constructs. We used site-directed mutagenesis to create αW493R, αW493C, βQ303A/βE304A/βD305A, γE348R, γE348C, and γR135Q/γK136Q/γR137Q/γR138Q con-

structs from linearized plasmids. cRNA was synthesized using SP6 RNA polymerase (mMessage mMachine, Ambion, Austin, TX). The γ-subunits were HA-tagged at their N termini to detect proteolytic fragments using anti-HA antibody (Covance) and immunoblotting of oocyte lysates.

For surface biotinylation and cysteine cross-linking, groups of 80–120 oocytes were coinjected with cRNA encoding WT or mutant ENaC subunits α, β, and γ and incubated overnight in modified Barth's solution (MBS), 85 mM NaCl, 1 mM KCl, 2.4 mM $NaHCO_3$, 0.82 mM $MgSO_4$, 0.41 mM $CaCl_2$, 0.33 mM $Ca(NO_3)_2$, 16.3 mM Hepes, and 10 μM amiloride at pH 7.4. 24 h after microinjection, oocytes were washed three times in MBS, followed by an incubation for 2 min at room temperature either in MBS only or in MBS containing the methanethiosulfonate cross-linker 1,2-ethanediyl bismethanethiosulfonate (M2M 5.2 Å, Toronto Research Chemicals) at 200 μM. Oocytes were washed three times, chilled on ice for 10 min, and then washed three times with MBS (pH 8.3) before biotinylation. Each group of oocytes was biotinylated for an hour with 1 mg/ml sulfo-NHS-biotin in MBS (pH 8.3), while gently tumbling at 4 °C. After biotinylation, oocytes were washed three times. Oocytes were lysed in 20 mM Tris, 50 mM NaCl, 50 mM NaF, 10 mM β-glycerophosphate, 5 mM $Na_2P_2O_7$, 1 mM EDTA at pH 7.4 containing protease inhibitors (Complete, Roche Applied Science). Oocytes were lysed by passing them twice through a 27½-gauge needle. Cell lysates were centrifuged at 4 °C at 3200 rpm to separate supernatants from cell pigments and debris. Supernatants were then collected and transferred into new tubes and centrifuged at 4 °C at 14,000 rpm to pellet membrane fractions. Membrane fractions were then solubilized in 50 mM Tris, 100 mM NaCl, 1% Triton X-100, 1% Nonidet P-40, 0.2% SDS, 0.1% sodium deoxycholate, 20 mM NaF, 10 mM $Na_4P_2O_7$, 10 mM EDTA, and protease inhibitor mixture at pH 7.5. Solubilized membrane fractions were incubated overnight with 100 μl of prewashed neutravidin beads (Pierce), while gently tumbling at 4 °C. Samples were washed twice with 500 mM NaCl, 50 mM Tris at pH 7.5, and once with 150 mM NaCl, 50 mM Tris at pH 7.5. Samples were then incubated at 96 °C for 5 min and separated by SDS-PAGE in a 7.5% acrylamide gel. Samples were transferred to a nitrocellulose membrane, which was then probed with the anti-αENaC mAb UNC1 19.2.1 recognizing an N-terminal epitope of human αENaC that was produced by the University of North Carolina Immunology Core Facility (40). Bands of anti-α-ENaC were detected by applying IRDye 680-conjugated goat anti-mouse IgG (Invitrogen) or IRDye 800-conjugate goat anti-rabbit IgG (Rockland Immunochemicals) and imaged using an Odyssey infrared imaging system (LI-COR Biosciences).

Electrophysiological Measurements—Recordings of amiloride-sensitive sodium currents were measured as described (26). Harvested oocytes were maintained in MBS, 85 mM NaCl, 1 mM KCl, 2.4 mM $NaHCO_3$, 0.82 mM $MgSO_4$, 0.41 mM $CaCl_2$, 0.33 mM $Ca(NO_3)_2$, 16.3 mM Hepes, and 10 μM amiloride at pH 7.4. For each construct, WT, or mutant channel, oocytes were coinjected with 0.3 ng of each cRNA encoding ENaC subunits α, β, and γ. 24 h after microinjection, two electrode voltage clamping was performed using a Geneclamp amplifier (Axon Instruments) in a constant perfusion system. Oocytes were voltage-clamped at −100 mV. Currents were digitized and recorded using a Digidata 1200 A/D converter (Axon Instruments) and AxoScope software. Recorded traces were analyzed using the pCLAMP software. Recordings were initiated in the presence of 10 μM amiloride. Following amiloride wash, basal currents were recorded in frog Ringer's solution, 2.5 mM KCl, 2.5 mM $CaCl_2$, 120 mM NaCl, and 10 mM Hepes at pH 7.35, to obtain I_{Na}. Results are from 5 to 6 oocytes per experimental group, repeated in 2–4 separate batches of oocytes.

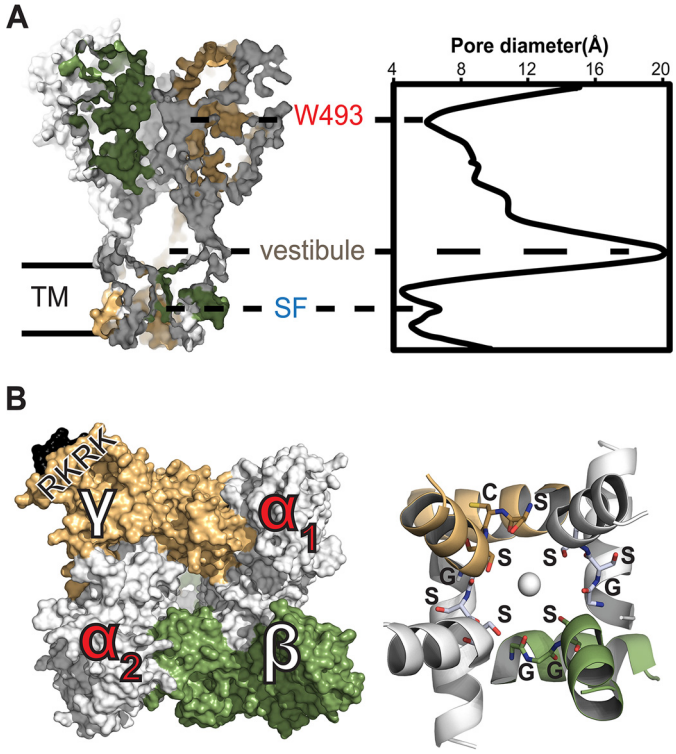

FIGURE 1. **Heterotetramer $\alpha_1\beta\alpha_2\gamma$ model of ENaC.** *A, left,* side view, surface-rendering representation of intersubunit topology. *Right,* pore geometry of the channel calculated by HOLE (60). Constrictions along the pore axis are labeled at Trp-493, an extracellular site of gain-of-function, and the selectivity filter (*SF*) in the transmembrane helical bundle. Extracellular vestibule along the pore spans the widest region in the channel. *B, left,* top view, extracellular surface of intersubunit interfaces. The trypsin cleavage site is colored *black* and labeled RKRK on the γ-subunit. *Right,* bottom view, schematic representation of the helical bundle formed by the transmembrane domain TM2 based on the open state of cASIC (Protein Data Bank code 4NTY). The selectivity filter residues αGSS, βGGS, and γSCS are labeled on the structure and shown as *sticks*. A serine quartet surrounds a hypothetical sodium ion on the channel pore axis.

Results

Quaternary Architecture of ENaC Tetramer $\alpha_1\beta\alpha_2\gamma$—In our $\alpha_1\beta\alpha_2\gamma$ model, ENaC subunits are symmetrically arranged around the channel pore axis (Fig. 1*A*). Each subunit forms contacts at intersubunit interfaces that stabilize the complex by inter-residue interactions. Although the different subunits share a common topology of highly conserved domains, such as the palm and β-ball domains in the core of each subunit, slight differences in sequence result in unique intersubunit interfaces (Fig. 2). Intersubunit contacts span the transmembrane domains in addition to extracellular domains, such as the knuckle-knuckle and knuckle-finger interdomain interactions. Most stabilizing intrasubunit contacts occur in the core region,

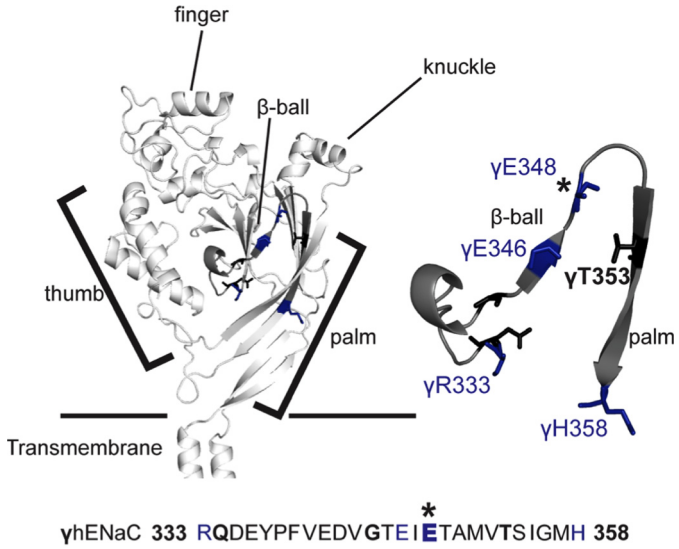

FIGURE 2. **Sequence alignment of interfacial residues in the palm and β-ball domains.** Alignment of sequences from the palm and β-ball domains of cASIC subunit and the α-, β-, and γ-subunits of ENaC indicates variable positions in loops connecting secondary structures. Highly conserved sequences are in boldface and colored in *black* and variable positions are colored in *blue*. Highlighted sequences are superimposed on cASIC crystal structure (Protein Data Bank code 2QTS). Experimentally tested Glu-348 is marked with an *asterisk*.

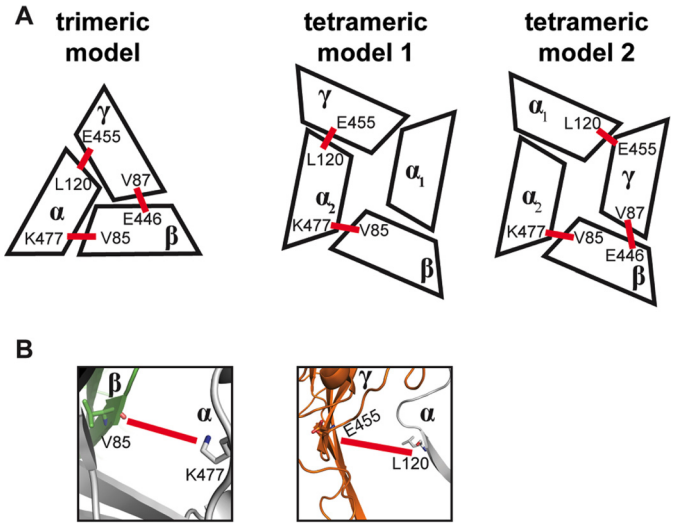

FIGURE 3. **Comparison of tetrameric interfaces with a previously validated trimeric interface.** *A*, schematic representations of a trimeric interface previously validated by cross-linking (35) and two previously proposed tetrameric configurations from functional studies of covalently linked concatemers (16). Cross-linking data from Collier *et al.* (41) suggest a trimeric clockwise topology of αγβ (35). These data also agree with two coexisting functional tetrameric configurations. Intersubunit angles vary slightly between trimer and tetramer models, resulting in slightly different interfaces as follows: in clockwise order, αβ, βγ, and γα, in addition to two unique interfaces to tetramers $\alpha_1\alpha_2$ and $\alpha_1\gamma$. *B*, schematic representation of $\alpha_2\beta$ and $\alpha_2\gamma$ interfaces in the tetramer model $\alpha_1\beta\alpha_2\gamma$. Shown as *sticks*, βV85 can cross-link with αLys-477, and γGlu-455 can cross-link with αLeu-120. Cross-linkers are represented as *red bars*.

with the largest surface area spanning the palm and β-ball domains (Fig. 2). ENaC subunits assemble by forming critical intersubunit interactions. These contacts include knuckle-finger and finger-finger interdomain interactions. The insertion of a second α-subunit changes the intersubunit angle from 120° in the crystallized trimeric configuration of cASIC to 90° in the tetramer model. Consequently, the modes of assembly of the pore-lining domains, TM1 and TM2, are slightly different between the trimeric and tetrameric configurations. Therefore, the conductive pore of ENaC can adopt somewhat different structures depending on the oligomeric state of the channel. In contrast, both oligomeric states result in a selectivity filter with a comparable constriction size of ~4 Å (Fig. 1*A*).

Similar to other multisubunit ion channels, the biophysical features of the heterotetramer's pore are determined by the geometric complementarity between subunits as the complex assembles from its monomers. Consequently, the pore contains fenestrations in the extracellular region occupied by water, ions, and small molecules such as amiloride or benzamil that can block the pore. Conversely, constrictions in the channel are formed by unique intersubunit contacts, such as the interfaces formed by the knuckle domains, where the site of the disease-causing mutation αW493R resides (Fig. 1*A*). Substitutions of this tryptophan to arginine, lysine, cysteine, or glutamic acid activate the channel (8). Therefore, the structural organization created by intersubunit interactions can play key functional roles in activating ENaC or stabilizing closed states of the channel. Finally, the gate and the selectivity filter of the channel form the narrowest region along the pore (Fig. 1*B*). Our structural model of ENaC heterotetramer agrees with previously published cross-linking data (41). At the $\alpha_2\beta$ interface, αLys-477 is in close proximity to cross-link with βV85. Similarly, at the $\alpha_2\gamma$ interface, αLeu-120 can cross-link with γGlu-455 (Fig. 3, *A* and *B*).

Asymmetry in Arg-493 Dynamics in the Knuckle Domains of the α_1- and α_2-Subunits—To investigate the effect of the gain-of-function mutation αW493R on the structural dynamics of ENaC, we performed DMD simulations of ENaC tetramer $\alpha_1\beta\alpha_2\gamma$. From our simulations, we predicted key inter-residue interactions. We tested these predictions by site-directed mutagenesis and electrophysiology recordings of oocytes. In our model, ENaC subunits are arranged in $\alpha_1\beta\alpha_2\gamma$ clockwise order such that α_1 complements β and β complements α_2. Therefore, this model defines interactions by Trp-493 in each α-subunit to be physiochemically distinct. Our homology model for the α-subunit derived from the cASIC crystal structure positions the Trp-493 rotamer in a pocket inside the knuckle domain cavity, which is geometrically constrained or stabilized by two phenylalanine residues Phe-280 and Phe-503 (Fig. 4). Substituting Trp-493 with an arginine reveals inter-residue interactions that can be either polar through H-bonding by backbone and side chain atoms or non-polar through the hydrophobic side chain of arginine.

Based on DMD simulations, we identified binding poses of the α_1Arg-493 rotamer buried in the knuckle domain pocket of the α_1-subunit at the $\alpha_1\beta$ interface. We analyzed the backbone dynamics of the knuckle domain by computing the root mean square fluctuations (RMSF) of Cα atoms. We found that the RMSF of the Arg-493 mutant knuckle domain in the α_1 subunit are increased compared with those of the WT channel (Fig. 5*B*),

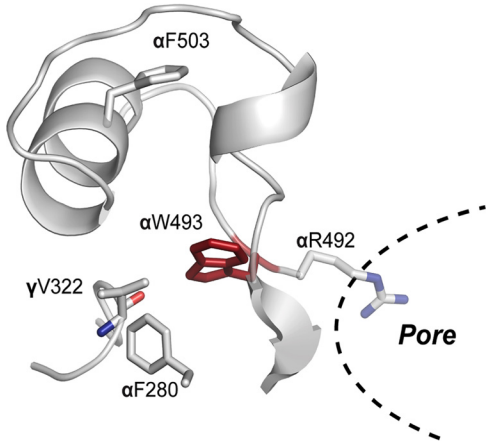

FIGURE 4. **Trp-493 binding pocket in a homology model of αENaC knuckle domain in $\alpha_1\beta\alpha_2\gamma$ tetramer.** Indole ring of Trp-493 is embedded inside the knuckle domain's cavity. Stabilizing phenylalanines Phe-280 and Phe-503 geometrically confine the pocket. Additional polar interactions stabilize the Trp-493's binding pose like γVal-322 from the neighboring γ-subunit. Trp-493 is connected to the pore-lining residue Arg-492 through the peptide chain.

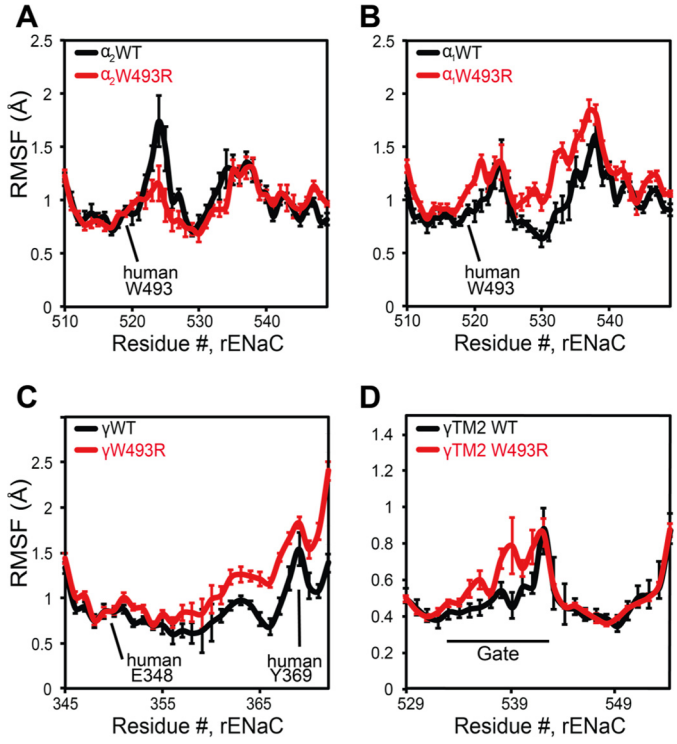

FIGURE 5. **Structural dynamics modulation in $\alpha_1\beta\alpha_2\gamma$ by W493R gain-of-function.** RMSF of Cα atoms in the α- and γ-subunits are from nine different 50-ns DMD trajectories; standard error is plotted for each residue. RMSF analysis is applied on equilibrated trajectories after discarding the first 5 ns. *A* and *B*, W493R destabilizes the knuckle domain of the α_1-subunit near the Trp-493 site. However, in the α_2-subunit, dynamics are slightly stabilized due to electrostatic interactions between α_2Arg-493 and γGlu-348 at the $\alpha_2\gamma$ interface. *C*, changes in dynamics of the γ-subunit propagate along a β-strand and enhance fluctuations of a loop, containing the signaling tyrosine Tyr-369, at the extracellular-transmembrane interface that communicates the activation signal (*D*); thus, fluctuations around the gate region containing the selectivity filter increase slightly.

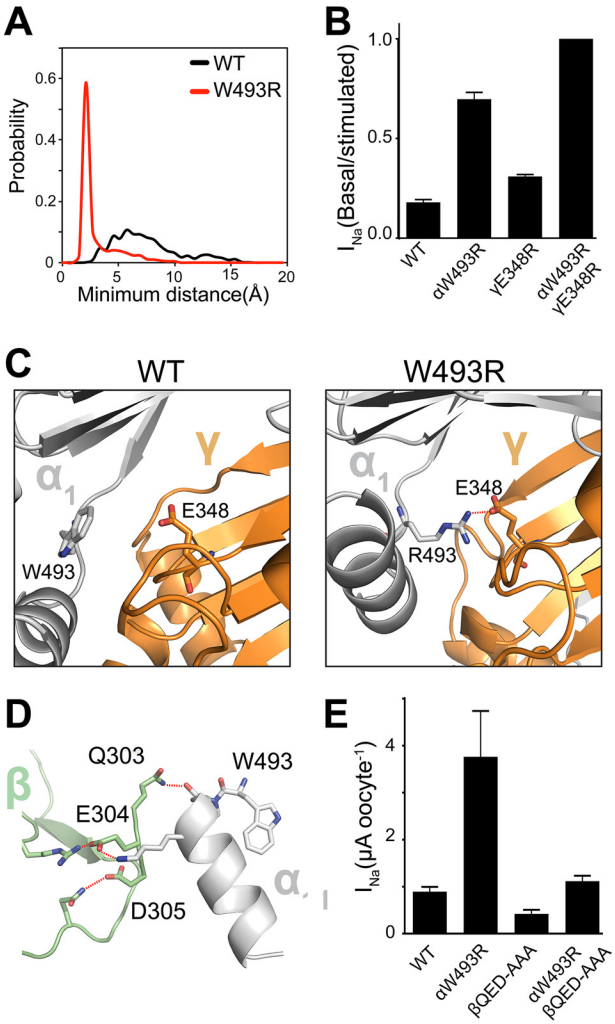

FIGURE 6. **W493R rewires intersubunit interactions.** *A*, DMD simulations indicate an electrostatic interaction between α_2Arg-493 (*red*) and γGlu-348 that is absent in the WT α_2-subunit (*black*). Inter-residue interactions are quantified by a histogram of minimum distance between α_2Arg-493 and γGlu-348. *B*, ENaC currents measured in oocytes injected with cRNA of WT and mutant ENaC subunits; basal current is normalized to trypsin-stimulated current to reflect basal activation. Perturbing the electrostatic interaction by the double mutant γE348R/αW493R channels shows no measurable population of near-silent channels, shown by lack of activation by trypsinization ($n = 18$, $p < 0.0001$). *C*, schematic representation of snapshots from DMD simulations at the $\alpha_2\gamma$ interface. Trp-493/Arg-493 in the α_2-subunit (*light gray*) and Glu-348 in the γ-subunit (*orange*) are shown as *sticks*, and hydrogen bonding between γGlu-348 and α_2Arg-493 is shown by *red dashed lines*. *D*, hydrogen bond network at the $\alpha_1\beta$ intersubunit interface by the acidic patch ^{303}QED^{305} in the β-subunit with the knuckle domain in the α_1-subunit. *E*, amiloride-sensitive current measured in oocytes. Neutralizing the acidic patch by alanine substitutions decreases W493R activation by ~2-fold ($n = 12$, $p = 0.002$). β^{303}AAA^{305} slightly inhibits WT ENaC ($n = 12$, $p = 0.008$).

possibly due to reconfiguration of the knuckle domain pocket, in which arginine and tryptophan adopt slightly different geometries. Interestingly, the α_2Arg-493 structural dynamics appear to be different from WT in the opposite α-subunit that forms an interface with the γ-subunit. In contrast, fluctuations are slightly decreased in the opposite α_2-subunit (Fig. 5*A*) due to stable electrostatic intersubunit interactions of α_2Arg-493 with neighboring acidic residues such as γGlu-348 and γGlu-346 (Fig. 6*C*).

Dissimilarity in the backbone dynamics of the α-subunits enhances fluctuations of the γ-subunit in the palm domain around γGlu-348 (Fig. 5*C*). Altered dynamics in the γ-subunit allosterically propagate down the channel through β-sheets in the palm domain to γTyr-369. This tyrosine residue has been proposed previously to communicate extracellular signals to

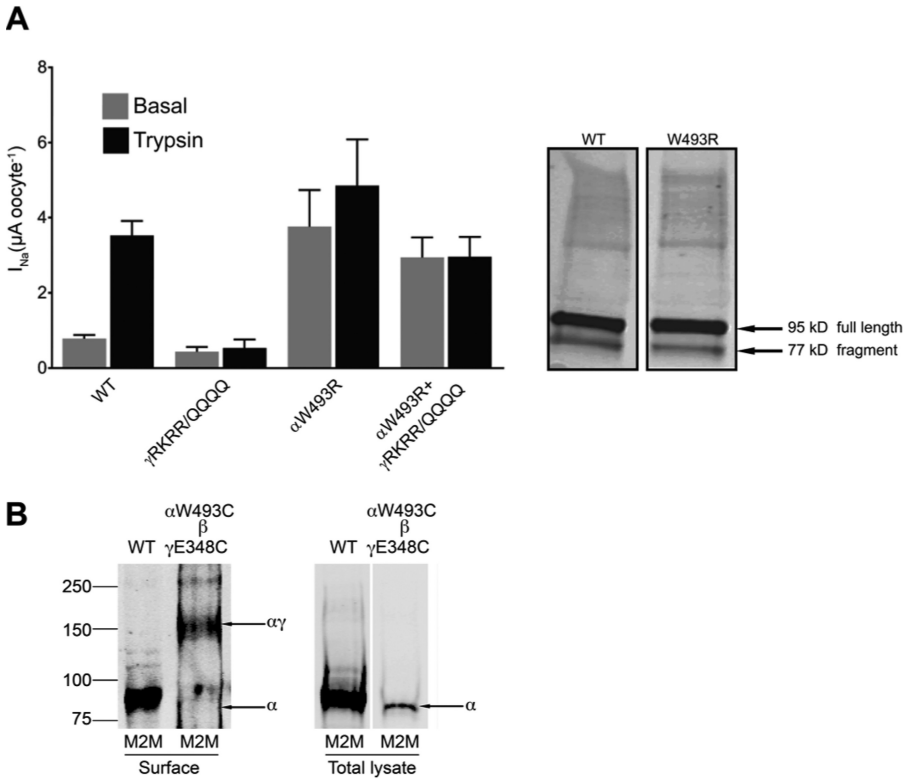

FIGURE 7. *A,* cleavage of the γ-subunit does not contribute to the gain-of-function in ENaC by αW493R. *Left,* amiloride-sensitive current measured in oocytes. Protease-insensitive γ^{135}QQQQ^{138} substitution prevents proteolytic activation by trypsin ($n = 12$, $p < 0.00001$). γ^{135}QQQQ^{138}/αW493R double mutant channels recapitulate the gain-of-function effect indicated by >3-fold increase in basal current and insensitivity to trypsinization ($n = 12$, $p = 0.0003$). *Right,* Western blots of the full-length and cleaved γ-subunit. Lysates from oocytes expressing the α-, β-, and HA-tagged γ-subunits were immunoblotted with anti-HA antibody. Marked by *arrows*, bands of full-length γ-subunit (95 kDa) and its cleaved form (77 kDa) are shown. Intensities of cleaved WT γENaC are comparable with the γENaC fragment in αW493R channels. *B,* cross-linking αW493C and γE348C using the cross-linker M2M at 200 μM. Cross-linking intact oocytes produced an ~175-kDa band that corresponds to the αγ dimer.

the transmembrane domain TM2 containing the selectivity filter, the rate-determining structure for sodium selectivity and permeation (41). These results show that extracellular fluctuations at intersubunit interfaces can allosterically propagate down the channel to the gating region.

Rewiring of Intersubunit Interactions Mediates αW493R ENaC Activation—The aspartic acids in the γ-subunit, γGlu-346 and γGlu-348, lie on a β-strand in the palm domain that is thought to stabilize the overall fold of ENaC subunits (9–11). In DMD simulations, γGlu-346 and γGlu-348 made statistically significant polar interactions with the side chain of α_2Arg-493 in the α_2-subunit (Fig. 6, *A* and *C*) (supplemental Movies 1 and 2). In addition to the di-aspartate moiety, other neighboring acidic residues make polar contacts with α_2Arg-493 at a lower frequency, ~10%. A histogram from time series of the minimum inter-residue distance between α_2Arg-493 and γGlu-348 indicates the stability of the α_2Arg-493 electrostatic interactions with γGlu-348 (Fig. 6*A*). Wild type α_2Trp-493 forms no significant contacts with γGlu-34; however, α_2Arg-493 forms stable electrostatic contacts indicated by an average contact distance of ~3 Å (Fig. 6*A*). To verify these interactions, we substituted γGlu-348 with an arginine and tested the effect of the electrostatic substitution γE348R on the function of wild type and αW493R ENaC in the heterologous expression system of *Xenopus* oocytes. The γE348R substitution cooperated with α_2W493R to fully activate the channel, indicated by no measurable response to activation by trypsin (Fig. 6*B*).

Because activation of ENaC by αW493R may be accounted for by an increase of cleavage in the γ-subunit, we collected lysates from oocytes that were used to measure ENaC currents and performed immunoblotting with an anti-HA antibody to detect N-terminal HA-tagged ENaC. We detected no difference in endogenous cleavage between wild type and αW493R γENaC (Fig. 7). To further validate the minimal role of proteolysis in the alternative activation mechanism by αW493R, we substituted the basic residues ^{135}RKRR^{138} in the γ-subunit with ^{135}QQQQ^{138}, thereby eliminating cleavage by furin. Furin cleavage at this site is thought to be a rate-determining step for proteolytic activation of ENaC and a pre-requisite step for the final cleavage events by extracellular proteases such as trypsin (9, 10). $\alpha/\beta/\gamma^{135}$QQQQ^{138} and αW493R/$\beta/\gamma^{135}$QQQQ^{138} showed no trypsin response (Fig. 7). Moreover, αW493R/β/γ^{135}QQQQ^{138} currents were comparable with the basal currents measured from αW493R/β/γ channels. In agreement with our hypothesis, these protease-resistant channels still recapitulated the gain-of-function phenotype in ENaC by αW493R. We perfused oocytes with 20 μg/ml trypsin to ensure full activation of proteolytically susceptible channels.

The double mutant channel γE348R/αW493R was insensitive to further stimulation by trypsin, indicating that the channel reached its maximal level of activity (Fig. 6*B*). These findings

suggest that intersubunit conformational changes induced by electrostatic interactions around the channel pore facilitate opening of the channel independent of the cleavage state of the channel. Because our DMD simulations and electrophysiology experiments provided supporting evidence for the functional role of electrostatic intersubunit interactions mediating ENaC activation, we hypothesized a functional role of the local electric field around α_1Arg-493 at the $\alpha_1\beta$ intersubunit interface. Therefore, we designed a mutant that neutralizes an acidic patch on the extracellular surface of the β-subunit. This mutant neutralizes the acidic charge on ^{303}QED^{305} by substituting QED to AAA. The QED patch is in direct contact with the knuckle domain of the α_1-subunit (Fig. 6*D*). We found from our DMD simulations formation of polar contacts by hydrogen bonding between the knuckle domain of the α_1-subunit and the QED patch in the β-subunit (Fig. 6*D*). The AAA mutation resulted in a slight inhibition of wild type ENaC. Conversely, ^{303}AAA^{305} β, when coexpressed with wild type γ and W493R α, negates the W493R gain-of-function effect by more than 2-fold (Fig. 6*E*). These findings support our hypothesis that the gain-of-function effect by W493R is mediated partly by changing intersubunit conformational changes, in addition to possibly altering the local electric field at the channel pore.

Cross-linking the αγ Interface at αW493C and γE348C—Our molecular dynamics simulations of ENaC tetramer model and electrophysiology data suggest an interaction between α_2Arg-493 and γGlu-348. To further validate the spatial proximity between the two residues, we used cysteine cross-linking. We introduced cysteine substitutions at these amino acid positions and applied the thiol-reactive cross-linker M2M to intact oocytes that expressed the cysteine mutant channels. We hypothesized that by cross-linking the introduced cysteines, αCys-493 and γCys-348, we can biochemically resolve the $\alpha\gamma$ dimer. In agreement with our hypothesis, cross-linking αW493C/β/γE348C channels produced a molecular species with a molecular mass of ~175 kDa that corresponds to the $\alpha\gamma$ dimer (Fig. 7*B*). This result supports our findings from molecular dynamics simulations and electrophysiology data that suggest an interaction between αW493R and γE348R in the tetrameric ENaC complex.

Allosteric Propagation of 493R's Asymmetric Dynamics in the Knuckle Domain to γTM2—Previous molecular dynamics simulations investigating the structural dynamics of the ASIC homotrimer suggested the importance of an allosteric pathway, in which twisting and vibrational motions in the knuckle, finger, and thumb domains communicate extracellular signals to the channel transmembrane domains (42). We probed this hypothesis using coevolution information of residues in the subunits of ion channels in the ENaC/Degenerin family. We used ASIC as a reference sequence and structure. Each node in the coevolution network represents a residue, and each edge is quantified by a mutual information metric that was calculated by the Mutual Information Server to Confer Coevolution (MISTIC) (43). We superimposed the mutual information edges on the ASIC structure and found a mutually evolved set of residues that line an allosteric structural path that is similar to the path previously proposed in the allosteric model of activation of ASIC (Fig. 8). High sequence conservation of residues on this path indicated a conserved allosteric network (Table 1). The path contains residues in TM2, in addition to γTyr-369 or Trp-288 in cASIC, that are involved in allosteric signaling by transmitting extracellular signals to the transmembrane domain by π-π stacking interactions (26, 44). Finally, a subset of that allosteric path is a linear path on the thumb domain, which is in contact with the β-ball and the knuckle domains (Fig. 8). Moreover, this coevolution analysis reveals possible allosteric mechanisms of a loss-of-function mutation in ENaC that is present in pseudohypoaldosteronism (PHA-1) patients. A highly conserved motif, HG, is mutated to HS in PHA-1 patients, altering the gating of ENaC, possibly by changing the conformational dynamics of the intracellular gate region (45). The HG motif, present in all members of the ENaC/Degenerin family, possesses a high number of coevolution contacts, in addition to exhibiting a high conservation score (Table 1). By integrating mutual information from coevolution and the structure of ASIC, we suggest that the allosteric parameters, which enable ENaC/Degenerin family to process extracellular clues, are encoded in the global fold of the channels.

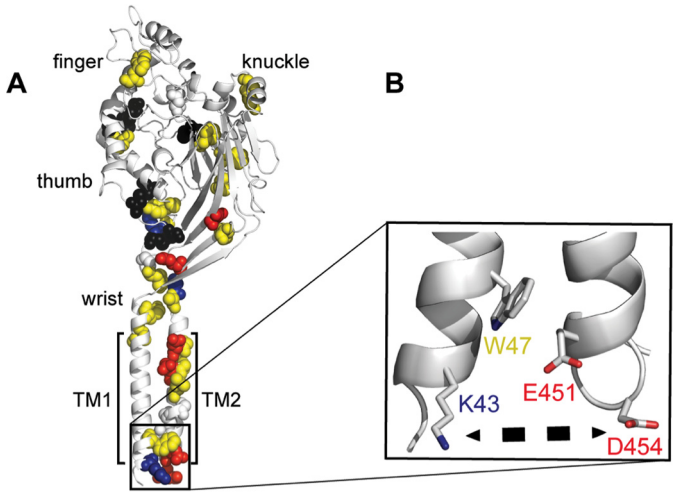

FIGURE 8. **Superposition of coevolving residues in the ENaC/Degenerin family on cASIC structure.** *A,* highly coevolving residues in the ENaC/Degenerin family computed from Mutual Information Server to Confer Coevolution (MISTIC) (42) superimposed on cASIC crystal structure. A spatially connected allosteric path of coevolving residues lines the thumb, knuckle, and the transmembrane spanning domain TM2. *B,* zooming in on a specific coevolving interaction between Lys-43 and Asp-454, which may stabilize the transmembrane structure by polar interactions. Charged residues are colored in *blue* (positive) and *red* (negative). Cysteines in disulfide bridges are colored in *black*. Hydrophobic residues are colored in *yellow*.

From our DMD simulations, we suggest a rewiring in the αW493R mutant inter-residue interaction network, mostly mediated by H-bonding and possibly salt bridges, to propagate from the knuckle domain of the α-subunit to the palm domain of the γ-subunit. The palm domain extends to a signaling tyrosine, γTyr-369, which is in contact with the transmembrane domain TM2 that facilitates channel gating (Fig. 9). Dynamics information derived from DMD simulations of ENaC heterotetramer suggests an allosteric model for W493R's gain-of-function effect, in which local fluctuations of the Arg-493 rotomeric ensemble drive differential dynamics in the α-subunits. Arg-493 in the α_1-subunit maintains binding poses that are mostly

TABLE 1

List of residues in cASIC with highest number of coevolution contacts

From the MISTIC analysis, the top 5% coevolving residues include highly conserved cysteine residues involved in disulfide bridges stabilizing the fold of subunits in the ENaC/Degenerin family. Trp-288 or Tyr-369 in γENaC, which is crucial for communicating allosteric signaling between the extracellular region and the transmembrane domains (20, 37), has a large number of 22 coevolution contacts. Highly conserved Gly-30 in the HG motif implicated in the PHA-1 disease also has a high coevolution contact number, 25, suggesting the structural importance of these allosteric sites in mediating the channel function in the ion channel family. A coevolution contact is considered significant by the MISTIC according to a z-score of >6.5 (36). Highly conserved cysteines are shown in boldface; the allosteric residue W288 is shown in blue; the disease-linked residue G30 is shown in red.

Residue index	Number of coevolved contacts	Conservation score
C195	**19**	**3.7991**
C336	**19**	**3.6269**
C291	**20**	**3.7717**
C309	**20**	**3.7885**
K423	20	0.489
G436	20	2.1345
L440	20	1.5609
P89	21	3.0472
C94	**21**	**3.6246**
W288	**22**	**0.8797**
D454	22	1.2401
W47	23	3.8197
C324	**23**	**3.7747**
C362	**23**	**3.707**
G435	24	2.3952
G443	24	2.325
G30	**25**	**2.0342**
C366	**26**	**3.7209**
S445	27	1.9637
G289	28	1.476
E451	30	2.0792
Q421	33	1.065
F22	35	1.9925

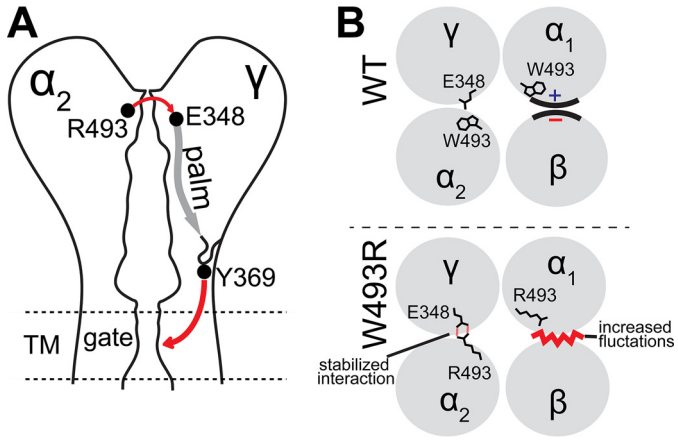

FIGURE 9. **Allosteric model of activation of ENaC by αW493R.** *A*, path of allosteric signaling mapped on a schematic diagram of the $\alpha_2\gamma$ interface. Initiation of activation signal is mediated by an electrostatic stabilizing interaction between α_2Arg-493 and γE348; the signal is then transmitted through a β-strand in the palm domain reaching a signaling loop. Loop fluctuations are predicted to enhance fluctuations in the gate region by γTyr-369 through π-π stacking interactions at the palm-transmembrane interface. *B*, top view of intersubunit interfaces. Fluctuations in hydrogen bonding network at WT $\alpha_1\beta$ interface (*top*) are increased at the mutant interface (*bottom*). Structural dynamics at the mutant $\alpha_2\gamma$ interface (*bottom*) are stabilized by electrostatic interactions between γGlu-348 and α_2Arg-493.

embedded inside the knuckle domain cavity. Consequently, the knuckle domain of the α_1-subunit in the mutant channel is slightly destabilized compared with the dynamics of wild type α_1 (Fig. 9). Moreover, the electrostatic interactions between α_2 and γ stabilize the $\alpha_2\gamma$ interface. We have used electrophysiology experiments to test the functional effects of perturbing these intersubunit interactions. The proposed model of the structural dynamics induced by W493R supports previous findings from structure-function studies that emphasize the contribution of intersubunit conformational changes in the extracellular vestibule to the structural and dynamic activation determinants of ENaC (41, 46).

Discussion

We propose a structural model of activation of the epithelial sodium channel by the pathological gain-of-function mutation αW493R. By integrating computational and experimental approaches, we identified critical intersubunit interactions that mediate allosteric activation of the channel. First, we revisit the previously suggested model of activation by αW493R, in which proteolytic cleavage in the α-subunit was found not to contribute to the gain-of-function of the channel (8). We further expand this model by showing that the gain-of-function by αW493R is independent of the cleavage state of the γ-subunit, which is considered the rate-determining step of proteolytic activation (9, 10). Our structural model of the heterotetramer $\alpha_1\beta\alpha_2\gamma$ of ENaC gives atomistic insight into the allosteric determinants that mediate channel activation.

The stoichiometries of ASICs, ENaCs, and other members in the ENaC/Degenerin family have been under debate. FMRFamide gated FaNaCh has been shown to assemble as a homotetramer (47). Functional approaches suggest tetrameric and trimeric assemblies of different ASIC subunits. ASIC1a and ASIC2a can form trimers of flexible stoichiometries 2:1 and 1:2 (48). However, ASIC1a, ASIC2a, and ASIC2b can form heterotetramers (49). Crystal structures of ASIC suggest a homotrimeric architecture (9–11). ASIC and ENaC subunits can assemble to form hybrid channels with novel functional characteristics (12). *In vitro* studies show heterotrimerization of ENaC (19). Conversely, functional data suggest a heterotetrameric configuration $\alpha_1\beta\alpha_2\gamma$ of ENaC. $\alpha_1\beta\alpha_2\gamma$ has been validated from structure-function characterization of ENaC oligomers using covalently linked concatemers (21). In addition, a heterotetrameric stoichiometry 2α:1β:1γ has been previously determined from epithelial cell lysates extracted from rabbit colon epithelial cells and cultured kidney cells (22). It is evident that the structural plasticity in the ENaC/Degenerin family facilitates formation of channels with diverse functionalities. However, it remains a challenge to reconcile structural data of ENaC assembly from *in vitro* studies with functional data of physiologically relevant oligomeric interfaces of the channel. The structural plasticity in the assembly of subunits of ion channels is not unique to the ENaC/Degenerin family. The potassium channel KCNQ1 has been crystallized as a trimer and as a tetramer (50). The extracellular domain of the ligand-gated ion channel GLIC has been crystalized as a pentamer and as a hexamer (51). Similar to ENaC, MscL is a mechanosensitive ion channel, which is activated by changes in the elastic energy stored in the lipid bilayer (52–54). MscL forms tetramers, pentamers, and hexamers (52, 55). An elastic model of MscL suggests that different oligomeric states can

shape the gating energy landscape and facilitate the contribution of membrane deformation energetics to the activation of the channel (55).

Rauh *et al.* (8) have suggested that ENaC gain-of-function by αW493R is mediated partly (~40%) by a decrease in sodium self-inhibition of ENaC. Self-inhibition is an inhibitory response of ENaC to sodium binding to the extracellular acidic surfaces at high sodium concentrations that limits conformational changes that shift the conformational equilibrium of the channel toward open states. By releasing inhibitory peptides from the α- and γ-subunits, extracellular proteases are thought to relieve the oligomeric complex from inhibitory interactions that stabilize the closed state of the channel. In addition, chloride ions inhibit ENaC by binding at extracellular intersubunit interfaces (41). Chloride binding, proteolysis, and sodium self-inhibition seem to induce a common functional perturbation altering the probability of occupying the closed state of the channel. Similarly, αW493R activates ENaC by perturbing inter-residue interactions that stabilize the closed state of the channel. Rauh *et al.* (8) substituted αTrp-493 with Arg, Lys, Cys, and Glu, and all of these substitutions activated the channel, suggesting the importance of αTrp-493 in stabilizing the closed state of the channel. We expand this model to include the role of αW493R in modulating intersubunit interactions as well as perturbing the dynamics of the knuckle domain. Recently, by cross-linking intersubunit interfaces, Gwiazda *et al.* (56) have shown the functional importance of the knuckle domain in ASIC. Moreover, active state stabilization by electrostatics has been shown in the erythromelalgia-causing gain-of-function mutation Q875E in the voltage-gated sodium channel Nav1.7 (57).

We have used the functionally validated heteromeric configuration of ENaC as a template for building a molecular model of ENaC tetramer. We tested our model using the experimentally characterized gain-of-function mutation αW493R. By probing the structural dynamics mediating the activation of the channel, our study suggests a dynamics-driven model for the previously established functional role of the extracellular domains that participate in sodium and chloride binding and undergo proteolytic cleavage. We used DMD simulations to refine and simulate the molecular model generated by symmetric docking. Our experimentally supported computational approach predicts a functional role of intersubunit structural dynamics mediating the gain-of-function effect of the disease-causing mutation αW493R. DMD simulations highlight the role of electrostatic interactions in modulating the intersubunit fluctuations triggered by the knuckle domain dynamics. Moreover, extracellular fluctuations are predicted to propagate through β-strands in the palm domain, reaching the signaling tyrosine γTyr-369 that contacts TM2, the sodium permeation rate-determining structure (58). We have shown previously that changing this tyrosine to a lysine slightly slows down the rate of proteolytic activation (26).

Proteolytic activation of the channel relieves inhibitory intrasubunit and possibly intersubunit interactions. To examine whether this mechanism applies to the αW493R's mode of action, we created an uncleavable mutant of the γ-subunit, and complementary to previous findings, we found that αW493R's mechanism of action is largely independent of proteolysis. Furthermore, αArg-493 is predicted in one α-subunit to interact with γGlu-348. By perturbing this interaction by changing Glu-348 to Arg-348, we fully activated αW493R channels and further decreased the pool of near-silent channels. We further validated the predicted inter-residue interaction by cysteine cross-linking. Interestingly, the examined electrostatic interaction exists in the tetramer model and is absent in our ENaC trimer models αβγ and αγβ. We have built models for the two possible trimeric configurations of ENaC, αβγ, and αγβ, using the crystallized homotrimeric topology of ASIC. Intersubunit angles differ slightly between trimeric and tetrameric interfaces. However, small differences in intersubunit orientation can rewire some inter-residue interactions.[4] The suggested electrostatic intersubunit interaction is predicted to fully activate the channel by inducing intersubunit conformational changes that possibly involve repulsive forces mimicking how proteolysis relieves inhibitory interactions. In agreement with our model, Collier *et al.* (41) showed that, by increasing the length of intersubunit cross-linkers, ENaC was further activated. Moreover, Edelheit *et al.* (59) have shown the functional importance of highly conserved charged residues on the extracellular surface of ENaC.

Lack of ENaC structural models for functionally characterized oligomers hinders progress in understanding the structural mechanism(s) underlying the activation of the channel. What are the structural and dynamic determinants that facilitate channel opening? How do gain- and loss-of-function mutations implicated in disease modulate the mechanism of action of the channel in processing extracellular and intracellular clues? These questions will remain largely unanswered until functional data from electrophysiology experiments can be explained mechanistically using experimentally validated structural models of the channel. Relying on experimental methods alone for structural determination of physiologically relevant oligomeric species is impractical due to current technical limitations in producing sufficient quantities of the different ENaC subunits and ensuring proper physiological conditions for *in vitro* oligomerization. Therefore, combining functional and computational approaches provides an alternative tool for building models that generate testable hypotheses regarding mechanisms of activation of WT and disease-causing forms of ENaC.

Plasticity in the structural dynamics of the epithelial sodium channel facilitates the functional flexibility to sense and respond to changes in the extracellular milieu. The versatility of the channel to process various signals is defined by the three-dimensional structure of its highly homologous subunits and their corresponding oligomers. Adapted by evolution, structural uniqueness confers functional specificity of signaling moieties such as proteolysis in the finger domains of the α- and γ-subunits. Our proposed dynamics-driven model for the gain-of-function in ENaC by αW493R highlights the role of the knuckle domain in facilitating activating intersubunit conformational changes. Other variants of ENaC implicated in dis-

[4] M. Shobair, P. Kota, and N. V. Dokholyan, unpublished data.

ease, such as γL511Q, require further understanding of their molecular mechanisms to build models for specific pharmacological targeting. The synergy between our functional findings and structural modeling enhances the understanding of the etiology of ENaC mutants.

Author Contributions—M. S., O. D., M. J. S., and N. V. D. designed the study, analyzed the data, and wrote the paper. P. K. performed homology modeling, and M. S. performed molecular docking and discrete molecular dynamics simulations shown in Figs. 1–6 and 8. Y. L. D. and M. S. performed site-directed mutagenesis and cRNA synthesis. H. H. performed voltage clamp electrophysiology experiments shown in Figs. 6 and 7. Y. L. D. performed Western blot experiments shown in Fig. 7. All authors reviewed the results and approved the final version of the manuscript.

Acknowledgments—We thank Dr. Howard Fried, Dr. Jhuma Das, Dr. Marino Convertino, and Tishan Williams for their helpful suggestions and discussions. We also acknowledge Dr. J. Riordan for providing us with cross-linking reagents and sharing his expertise on the biochemistry of cross-linking ion channels.

References

1. Bhalla, V., and Hallows, K. R. (2008) Mechanisms of ENaC regulation and clinical implications. *J. Am. Soc. Nephrol.* **19,** 1845–1854
2. Shehata, M. F. (2009) Regulation of the epithelial sodium channel [ENaC] in kidneys of salt-sensitive Dahl rats: insights on alternative splicing. *Int. Arch. Med.* **2,** 28
3. Baker, S. E., Wheatley, C. M., Cassuto, N. A., Foxx-Lupo, W. T., Sprissler, R., and Snyder, E. M. (2011) Genetic variation of αENaC influences lung diffusion during exercise in humans. *Respir. Physiol. Neurobiol.* **179,** 212–218
4. Azad, A. K., Rauh, R., Vermeulen, F., Jaspers, M., Korbmacher, J., Boissier, B., Bassinet, L., Fichou, Y., des Georges, M., Stanke, F., De Boeck, K., Dupont, L., Balascáková, M., Hjelte, L., Lebecque, P., *et al.* (2009) Mutations in the amiloride-sensitive epithelial sodium channel in patients with cystic fibrosis-like disease. *Hum. Mutat* **30,** 1093–1103
5. Howsham, C., and Danahay, H. (2014) in *Ion Channel Drug Discovery* (Cox, B., and Gosling, M., eds) pp. 135–155, Royal Society of Chemistry, London
6. Foxx-Lupo, W. T., Wheatley, C. M., Baker, S. E., Cassuto, N. A., Delamere, N. A., and Snyder, E. M. (2011) Genetic variation of the α subunit of the epithelial Na^+ channel influences exhaled Na^+ in healthy humans. *Respir Physiol. Neurobiol.* **179,** 205–211
7. Handschick, M., Hedtfeld, S., and Tümmler, B. (2012) Frequency of the hyperactive W493R ENaC variant in carriers of a CFTR mutation. *J. Cyst. Fibros.* **11,** 53–55
8. Rauh, R., Diakov, A., Tzschoppe, A., Korbmacher, J., Azad, A. K., Cuppens, H., Cassiman, J. J., Dötsch, J., Sticht, H., and Korbmacher, C. (2010) A mutation of the epithelial sodium channel associated with atypical cystic fibrosis increases channel open probability and reduces Na^+ self- inhibition. *J. Physiol.* **588,** 1211–1225
9. Kota, P., García-Caballero, A., Dang, H., Gentzsch, M., Stutts, M. J., and Dokholyan, N. V. (2012) Energetic and structural basis for activation of the epithelial sodium channel by matriptase. *Biochemistry* **51,** 3460–3469
10. Hughey, R. P., Bruns, J. B., Kinlough, C. L., Harkleroad, K. L., Tong, Q., Carattino, M. D., Johnson, J. P., Stockand, J. D., and Kleyman, T. R. (2004) Epithelial sodium channels are activated by furin-dependent proteolysis. *J. Biol. Chem.* **279,** 18111–18114
11. Sheng, S., Carattino, M. D., Bruns, J. B., Hughey, R. P., and Kleyman, T. R. (2006) Furin cleavage activates the epithelial Na^+ channel by relieving Na^+ self-inhibition. *Am. J. Physiol. Renal Physiol* **290,** F1488–F1496
12. Harris, M., Garcia-Caballero, A., Stutts, M. J., Firsov, D., and Rossier, B. C. (2008) Preferential assembly of epithelial sodium channel (ENaC) subunits in *Xenopus* oocytes: role of furin-mediated endogenous proteolysis. *J. Biol. Chem.* **283,** 7455–7463
13. Kashlan, O. B., Boyd, C. R., Argyropoulos, C., Okumura, S., Hughey, R. P., Grabe, M., and Kleyman, T. R. (2010) Allosteric inhibition of the epithelial Na^+ channel through peptide binding at peripheral finger and thumb domains. *J. Biol. Chem.* **285,** 35216–35223
14. Baconguis, I., Bohlen, C. J., Goehring, A., Julius, D., and Gouaux, E. (2014) X-ray structure of acid-sensing ion channel 1-snake toxin complex reveals open state of a Na^+-selective channel. *Cell* **156,** 717–729
15. Dawson, R. J., Benz, J., Stohler, P., Tetaz, T., Joseph, C., Huber, S., Schmid, G., Hügin, D., Pflimlin, P., Trube, G., Rudolph, M. G., Hennig, M., and Ruf, A. (2012) Structure of the acid-sensing ion channel 1 in complex with the gating modifier Psalmotoxin 1. *Nat. Commun.* **3,** 936
16. Jasti, J., Furukawa, H., Gonzales, E. B., and Gouaux, E. (2007) Structure of acid-sensing ion channel 1 at 1.9 A resolution and low pH. *Nature* **449,** 316–323
17. Sherwood, T. W., Lee, K. G., Gormley, M. G., and Askwith, C. C. (2011) Heteromeric acid-sensing ion channels (ASICs) composed of ASIC2b and ASIC1a display novel channel properties and contribute to acidosis-induced neuronal death. *J. Neurosci.* **31,** 9723–9734
18. Meltzer, R. H., Kapoor, N., Qadri, Y. J., Anderson, S. J., Fuller, C. M., and Benos, D. J. (2007) Heteromeric assembly of acid-sensitive ion channel and epithelial sodium channel subunits. *J. Biol. Chem.* **282,** 25548–25559
19. Babini, E., Geisler, H. S., Siba, M., and Gründer, S. (2003) A new subunit of the epithelial Na^+ channel identifies regions involved in Na^+ self-inhibition. *J. Biol. Chem.* **278,** 28418–28426
20. Ji, H. L., Zhao, R. Z., Chen, Z. X., Shetty, S., Idell, S., and Matalon, S. (2012) δENaC: a novel divergent amiloride-inhibitable sodium channel. *Am. J. Physiol. Lung Cell. Mol. Physiol.* **303,** L1013–L1026
21. Firsov, D., Gautschi, I., Merillat, A.-M., Rossier, B. C., Schild, L. (1998) The heterotetrameric architecture of the epithelial sodium channel (ENaC). *EMBO J.* **17,** 344–352
22. Dijkink, L., Hartog, A., van Os, C. H., and Bindels, R. J. (2002) The epithelial sodium channel (ENaC) is intracellularly located as a tetramer. *Pflugers Arch.* **444,** 549–555
23. Stewart, A. P., Haerteis, S., Diakov, A., Korbmacher, C., and Edwardson, J. M. (2011) Atomic force microscopy reveals the architecture of the epithelial sodium channel (ENaC). *J. Biol. Chem.* **286,** 31944–31952
24. Butterworth, M. B., Weisz, O. A., and Johnson, J. P. (2008) Some assembly required: putting the epithelial sodium channel together. *J. Biol. Chem.* **283,** 35305–35309
25. Garty, H., and Palmer, L. G. (1997) Epithelial sodium channels: function, structure, and regulation. *Physiol. Rev.* **77,** 359–396
26. Kota, P., Buchner, G., Chakraborty, H., Dang, Y. L., He, H., Garcia, G. J., Kubelka, J., Gentzsch, M., Stutts, M. J., and Dokholyan, N. V. (2014) The N-terminal domain allosterically regulates cleavage and activation of the epithelial sodium channel. *J. Biol. Chem.* **289,** 23029–23042
27. Yin, S., Ding, F., and Dokholyan, N. V. (2010) in *Introduction to Protein Structure Prediction* (Rangwala, H., and Karypis, G., eds) pp. 453–476, John Wiley & Sons, Inc., New York
28. Ding, F., and Dokholyan, N. V. (2006) Emergence of protein fold families through rational design. *PLoS Comput. Biol.* **2,** e85
29. Webb, B., and Sali, A. (2014) Protein structure modeling with MODELLER. *Methods Mol. Biol.* **1137,** 1–15
30. Proctor, E. A., Ding, F., and Dokholyan, N. V. (2011) Discrete molecular dynamics. *Wiley Interdisciplinary Reviews. Comput. Mol. Sci.* **1,** 80–92
31. Ding, F., and Dokholyan, N.V. (2012) in *Computational Modeling of Biological Systems: From Molecules to Pathways* (Dokholyan, N. V., ed) pp. 55–73, Springer-Verlag, New York
32. Shirvanyants, D., Ding, F., Tsao, D., Ramachandran, S., and Dokholyan, N. V. (2012) Discrete molecular dynamics: an efficient and versatile simulation method for fine protein characterization. *J. Phys. Chem. B* **116,** 8375–8382
33. Ding, F., Tsao, D., Nie, H., and Dokholyan, N. V. (2008) *Ab initio* folding of proteins with all-atom discrete molecular dynamics. *Structure* **16,** 1010–1018
34. Proctor, E. A., Kota, P., Aleksandrov, A. A., He, L., Riordan, J. R., and Dokholyan, N. V. (2015) Rational coupled dynamics network manipula-

tion rescues disease-relevant mutant cystic fibrosis transmembrane conductance regulator. *Chem. Sci.* **6,** 1237–1246
35. Dagliyan, O., Shirvanyants, D., Karginov, A. V., Ding, F., Fee, L., Chandrasekaran, S. N., Freisinger C. M., Smolen, G. A., Huttenlocher, A., Hahn, K. M., and Dokholyan, N. V. (2013) Rational design of a ligand-controlled protein conformational switch. *Proc. Natl. Acad. Sci. U.S.A.* **110,** 6800–6804
36. Dagliyan, O., Proctor, E. A., D'Auria, K. M., Ding, F., and Dokholyan, N. V. (2011) Structural and dynamic determinants of protein-peptide recognition. *Structure* **19,** 1837–1845
37. Schneidman-Duhovny, D., Inbar, Y., Nussinov, R., and Wolfson, H. J. (2005) PatchDock and SymmDock: servers for rigid and symmetric docking. *Nucleic Acids Res.* **33,** W363–W367
38. Ramachandran, S., Kota, P., Ding, F., and Dokholyan, N. V. (2011) Automated minimization of steric clashes in protein structures. *Proteins* **79,** 261–270
39. Yin, S., Ding, F., and Dokholyan, N. V. (2007) Eris: An automated estimator of protein stability. *Nature Methods* **4,** 466–467
40. Gentzsch, M., Dang, H., Dang, Y., Garcia-Caballero, A., Suchindran, H., Boucher, R. C., and Stutts, M. J. (2010) The cystic fibrosis transmembrane conductance regulator impedes proteolytic stimulation of the epithelial Na^+ channel. *J. Biol. Chem.* **285,** 32227–32232
41. Collier, D. M., Tomkovicz, V. R., Peterson, Z. J., Benson, C. J., and Snyder, P. M. (2014) Intersubunit conformational changes mediate epithelial sodium channel gating. *J. Gen. Physiol.* **144,** 337–348
42. Yang, H., Yu, Y., Li, W. G., Yu, F., Cao, H., Xu, T. L., and Jiang, H. (2009) Inherent dynamics of the acid-sensing ion channel 1 correlates with the gating mechanism. *PLoS Biol.* **7,** e1000151
43. Simonetti, F. L., Teppa, E., Chernomoretz, A., Nielsen, M., and Marino Buslje, C. (2013) MISTIC: Mutual information server to infer coevolution. *Nucleic Acids Res.* **41,** W8–W14
44. Li, T., Yang, Y., and Canessa, C. M. (2009) Interaction of the aromatics Tyr-72/Trp-288 in the interface of the extracellular and transmembrane domains is essential for proton gating of acid-sensing ion channels. *J. Biol. Chem.* **284,** 4689–4694
45. Kucher, V., Boiko, N., Pochynyuk, O., and Stockand, J. D. (2011) Voltage-dependent gating underlies loss of ENaC function in Pseudohypoaldosteronism type 1. *Biophys. J.* **100,** 1930–1939
46. Kashlan, O. B., Blobner, B. M., Zuzek, Z., Tolino, M., and Kleyman, T. R. (2015) Na^+ inhibits the epithelial Na^+ channel by binding to a site in an extracellular acidic cleft. *J. Biol. Chem.* **290,** 568–576
47. Coscoy, S., Lingueglia, E., Lazdunski, M., and Barbry, P. (1998) The Phe-Met-Arg-Phe-amide-activated sodium channel is a tetramer. *J. Biol. Chem.* **273,** 8317–8322
48. Bartoi, T., Augustinowski, K., Polleichtner, G., Gründer, S., and Ulbrich, M. H. (2014) Acid-sensing ion channel (ASIC) 1a/2a heteromers have a flexible 2:1/1:2 stoichiometry. *Proc. Natl. Acad. Sci. U.S.A.* **111,** 8281–8286
49. Gao, Y., Liu, S. S., Qiu, S., Cheng, W., Zheng, J., and Luo, J. H. (2007) Fluorescence resonance energy transfer analysis of subunit assembly of the ASIC channel. *Biochem. Biophys. Res. Commun.* **359,** 143–150
50. Xu, Q., and Minor, D. L., Jr. (2009) Crystal structure of a trimeric form of the K(V)7.1 (KCNQ1) A-domain tail coiled-coil reveals structural plasticity and context dependent changes in a putative coiled-coil trimerization motif. *Protein. Sci.* **18,** 2100–2114
51. Nury, H., Bocquet, N., Le Poupon, C., Raynal, B., Haouz, A., Corringer, P. J., and Delarue, M. (2010) Crystal structure of the extracellular domain of a bacterial ligand-gated ion channel. *J. Mol. Biol.* **395,** 1114–1127
52. Liu, Z., Gandhi, C. S., and Rees, D. C. (2009) Structure of a tetrameric MscL in an expanded intermediate state. *Nature* **461,** 120–124
53. Wei, S. P., Li, X. Q., Chou, C. F., Liang, Y. Y., Peng, J. B., Warnock, D. G., and Ma, H. P. (2007) Membrane tension modulates the effects of apical cholesterol on the renal epithelial sodium channel. *J. Membr. Biol.* **220,** 21–31
54. Krueger, B., Haerteis, S., Yang, L., Hartner, A., Rauh, R., Korbmacher, C., and Diakov, A. (2009) Cholesterol depletion of the plasma membrane prevents activation of the epithelial sodium channel (ENaC) by SGK1. *Cell. Physiol. Biochem.* **24,** 605–618
55. Haselwandter, C. A., and Phillips, R. (2013) Connection between oligomeric state and gating characteristics of mechanosensitive ion channels. *PLoS Comput. Biol.* **9,** e1003055
56. Gwiazda, K., Bonifacio, G., Vullo, S., and Kellenberger, S. (2015) Extracellular subunit interactions control transitions between functional states of acid-sensing ion channel 1a. *J. Biol. Chem.* **290,** 17954–17966
57. Stadler, T., O'Reilly, A. O., and Lampert, A. (2015) Erythromelalgia mutation Q875E stabilizes the activated state of sodium channel Nav1.7. *J. Biol. Chem.* **290,** 6316–6325
58. Abi-Antoun, T., Shi, S., Tolino, L. A., Kleyman, T. R., and Carattino, M. D. (2011) Second transmembrane domain modulates epithelial sodium channel gating in response to shear stress. *Am. J. Physiol. Renal Physiol.* **300,** F1089–F1095
59. Edelheit, O., Ben-Shahar, R., Dascal, N., Hanukoglu, A., and Hanukoglu, I. (2014) Conserved charged residues at the surface and interface of epithelial sodium channel subunits–roles in cell surface expression and the sodium self-inhibition response. *FEBS J.* **281,** 2097–2111
60. Smart, O. S., Neduvelil, J. G., Wang, X., Wallace, B. A., and Sansom, M. S. (1996) HOLE: A program for the analysis of the pore dimensions of ion channel structural models. *J. Mol. Graph.* **14,** 354–360

Gain-of-Function Mutation W493R in the Epithelial Sodium Channel Allosterically Reconfigures Intersubunit Coupling

Mahmoud Shobair, Onur Dagliyan, Pradeep Kota, Yan L. Dang, Hong He, M. Jackson Stutts and Nikolay V. Dokholyan

J. Biol. Chem. 2016, 291:3682-3692.
doi: 10.1074/jbc.M115.678052 originally published online December 14, 2015